

# Topology and Toolpath Optimization-Inspired Toolpath Planning for Continuous Fiber Material Extrusion

Joseph R. Kubalak

Applied Research Laboratory, Pennsylvania State University

Corresponding author: [jrk6166@arl.psu.edu](mailto:jrk6166@arl.psu.edu)

## Abstract

Topology and orientation optimization (TOO) simultaneously designs part geometry and local material orientations to maximize structural performance, but the resulting designs must be interpreted for manufacturing. Due to strict adherence to the optimized geometry's boundaries, existing alignment-based material extrusion (MEX) slicers produce poor quality toolpaths (especially for continuous fiber-reinforced materials). Topology optimization-inspired design is a technique in which the optimized geometry is manually edited by a user to improve manufacturability while retaining structural performance. In this work, we adapt this concept to MEX toolpaths. Bézier splines are used as a toolpath planning primitive that are softly fit to the optimized design while ensuring highly continuous, well-aligned, and consistently spaced deposition paths. This representation also allows the user to manually edit the output toolpath (via spline control points) to tune it for manufacturability. Toolpaths are generated using the outlined method and compared to other alignment-based toolpath planning techniques.

## 1. Introduction

Especially for additive manufacturing (AM) processes that selectively pattern material (namely, material extrusion; MEX), the toolpath has a profound impact on structural performance [1]. The mechanical properties aligned with the deposition path (road) direction are significantly stronger than either the inter- [2] or intra-layer [3] bonds. This anisotropy becomes increasingly pronounced with reinforced (e.g., continuous fiber reinforced; CFR) materials, as the fiber inherently aligns with the deposition direction [4]. To maximize final part performance, the roads should be aligned to anticipated load paths (represented by an orientation field; Figure 1) everywhere in the geometry. However, there are manufacturing considerations that make this challenging to achieve, especially depending on the complexity of the geometry and its anticipated load paths. In addition to being well-aligned to load paths, an ideal toolpath should also address:

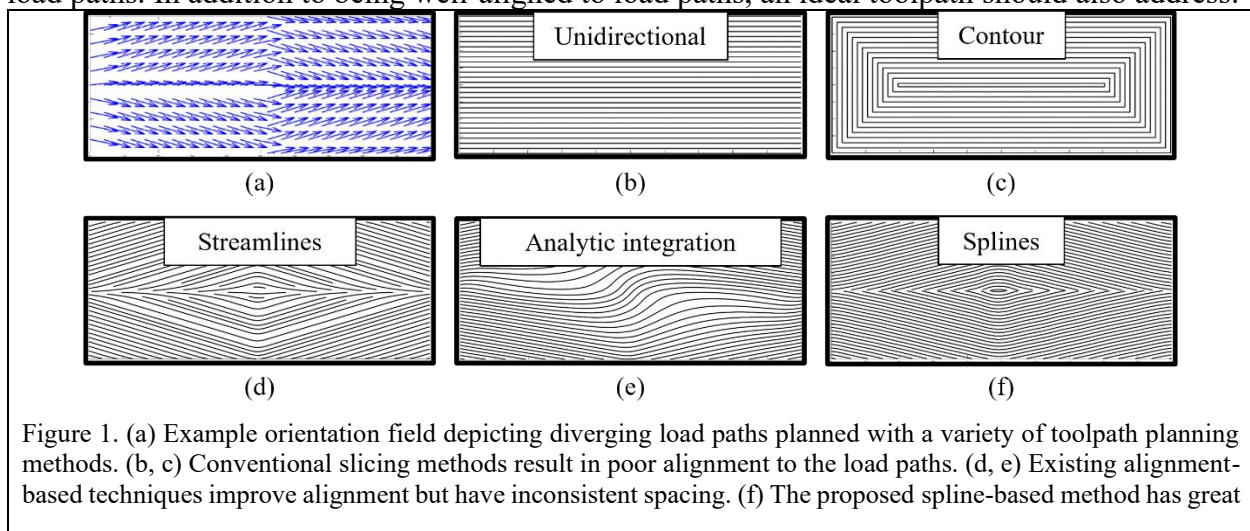


Figure 1. (a) Example orientation field depicting diverging load paths planned with a variety of toolpath planning methods. (b, c) Conventional slicing methods result in poor alignment to the load paths. (d, e) Existing alignment-based techniques improve alignment but have inconsistent spacing. (f) The proposed spline-based method has great

1. **Consistent road spacing.** A stereotypical raster pattern has perfectly uniform spacing between adjacent roads (Figure 1b). However, local variation in the road directions can cause imperfect packing and ultimately either over- or under-deposition (Figure 1d and Figure 1e). This internal porosity can significantly reduce mechanical performance, despite the improved alignment from the roads themselves.
2. **Connectivity and path length.** In the context of a neat or short fiber-reinforced (SFR) material, a large number of short roads can decrease deposition quality due to frequent extrusion start-stop commands. This characteristic is even more damaging for a CFR material, as there is often a minimum path length that can be printed [5]. Each individual path also requires a separate cutting operation, reducing overall fiber length.
3. **Material curvature constraints.** This aspect is less of a concern for neat or SFR materials, as the materials are often capable of rapid direction changes; however, with a CFR material, there is often a minimum achievable path curvature before the fiber is misplaced or damaged during deposition [6].

Although tailored toolpath alignment is largely unavailable in commercial slicing software, researchers have presented a number of solutions. Rezaie et al. and Li et al. graded the density of unit cells based on the density results from topology optimization (TO) [7], [8]. Ahsan and Khoda used a similar density map to deform a honeycomb infill pattern [9]. Zhang et al. presented a method that would partition a geometry and align the local infill pattern to the principal stress field [10]. Although these methods have demonstrated improved mechanical performance relative to conventional slicing algorithms, they often leave significant material in suboptimal orientations. Others have explored hierarchical toolpath planning methods that create local sparsity [11]. These have been demonstrated with CFR materials [12], but the path spacing is necessarily inconsistent. This renders the methods unsuitable for producing solid geometries.

Another common strategy is to interpret the anticipated load paths as a vector field and integrate it to form the toolpath. The most straight-forward is numerical integration, often by employing a streamline placement algorithm (Figure 1d) [13]–[17]. This technique results in explicit road alignment to the vector field and has been shown to correspondingly improve mechanical performance relative to more conventional toolpath planning methods. However, they often result in uneven spacing due to the iterative seeding and advection process [17]. This creates internal porosity and reduces material/fiber volume fraction. The methods also produce a significant number of short streamlines that are entirely unmanufacturable via a CFR material.

Alternatively, the vector field can be integrated analytically. The specific mechanism can vary (e.g., wave equation [18], [19], Poisson equation [20], and the heat method [21]), but the methods generally focus on creating a scalar field through which isosurfaces/isocontours can be populated. Although these methods can result in well-aligned roads, they often require preconditioning (i.e., modification) of the vector field to achieve good results [20]. Analytic integration techniques especially encounter difficulties with non-conservative vector fields [22]. Offending behaviors (e.g., non-zero curl) are often ignored during the integration process, which can result in poorly aligned roads with uneven spacing for even relatively simple orientation fields (e.g., Figure 1e).

In part, the shortcomings of existing alignment-based techniques come as a consequence of only softly fitting the toolpath to the orientation field and holding the geometry as an inflexible constant; no interpretation of the geometry is permitted, even when small modifications would dramatically improve toolpath quality. This paper applies the concept of topology optimized-inspired design (i.e., the results of TO are interpreted to improve manufacturability while retaining dominant features) to toolpath planning. To accomplish this goal, a primitive-based toolpath

planning method is proposed in which cubic Bézier splines are fit to a geometry and its anticipated load paths. This is similar to other recently published research that focuses on fitting splines to density-based TO results [23]. Here, those concepts are extended to the results of topology and orientation optimization (TOO) algorithms [24]; however, inputs could be generated using other methods (e.g., a manually-designed geometry’s principal stress field).

As opposed to rigidly adhering to the input geometry’s boundaries, toolpath continuity and manufacturability are held as the top priority. They are formulated as constraints under which alignment to the orientation field and geometric fidelity are maximized. Section 2 presents the splines-based toolpath planning methodology. Section 3 demonstrates the workflow and compares an example toolpath to existing alignment-based toolpath planning strategies. Preliminary CFR-MEX printing of a toolpath is also presented. Section 4 summarizes the contribution and outlines paths for future work.

## 2. Splines-Based Toolpath Planning

A schematic of the presented toolpath planning methodology is shown in Figure 2. From a provided set of inputs (a desired geometry and orientation field), the user draws a set of splines that constitute an initial toolpath. These manually-drawn splines are then algorithmically fit to the orientation field to maximize alignment with consideration for manufacturing constraints (e.g., fiber turning radius). The user is then able to continue editing the optimized splines before exporting them to a MEX process for fabrication.

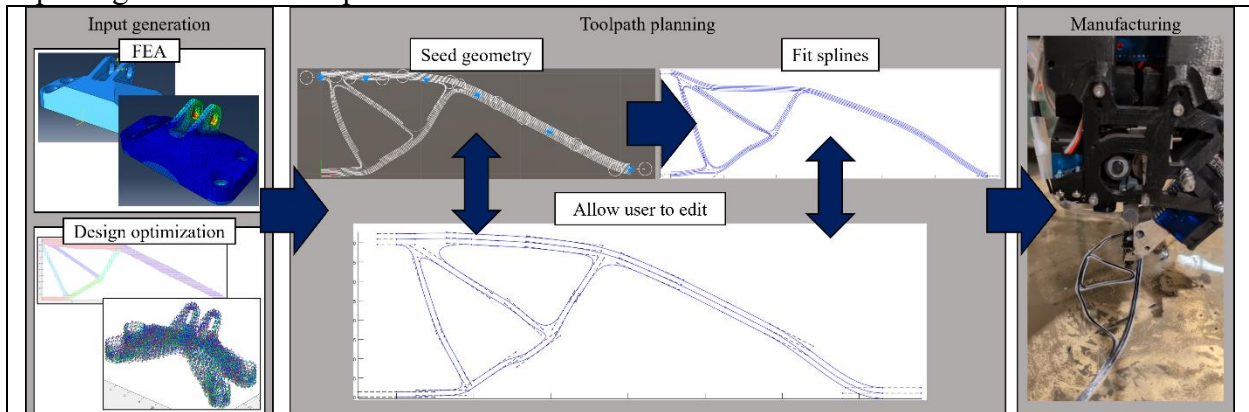


Figure 2. Schematic of the splines-based toolpath planning method. The user provides a geometry and orientation field (e.g., anticipated load paths) and seeds the geometry with a set of spline "families". These are fit to the orientation field. As necessary, the user can continue to edit the toolpath for manufacturability. Once prepared, the splines can be ordered and exported to a toolpath for manufacture.

Section 2.1 details the mathematics of the spline formulation, and Section 2.2 discusses the formation of spline “families” (i.e., a series of offset splines from a single set of control points) that serve to maintain consistent spacing, reduce computational expense, and improve user editability. Section 2.3 outlines the optimization method by which the splines are aligned to the orientation field. Once the user is satisfied with toolpath quality, the splines are ordered to minimize travel movements and fiber cutting (Section 2.4).

### 2.1. Spline Definition

A cubic Bézier spline consists of a number of segments, each defined by four control points ( $\mathbf{P}$ ). The position of the spline ( $\mathbf{x}$ ) along each segment ( $i$ ) is defined as shown in Equation 1.

$$\mathbf{x}_i(t) = (1 - t)^3 \mathbf{P}_{i,0} + 3(1 - t)^2 t \mathbf{P}_{i,1} + 3(1 - t) t^2 \mathbf{P}_{i,2} + t^3 \mathbf{P}_{i,3} \text{ where } 0 \leq t \leq 1 \quad (1)$$

An example spline is shown in Figure 3. Clearly, the spline explicitly travels through the first and last control point of each segment (i.e., the “knots”). In contrast, the spline does not necessarily

travel through the control points in the middle of each segment. Instead, the position of these control points (relative to their adjacent knots) affects the starting/ending direction of their respective spline segment. For this reason, they may be referred to as “tangent” control points.

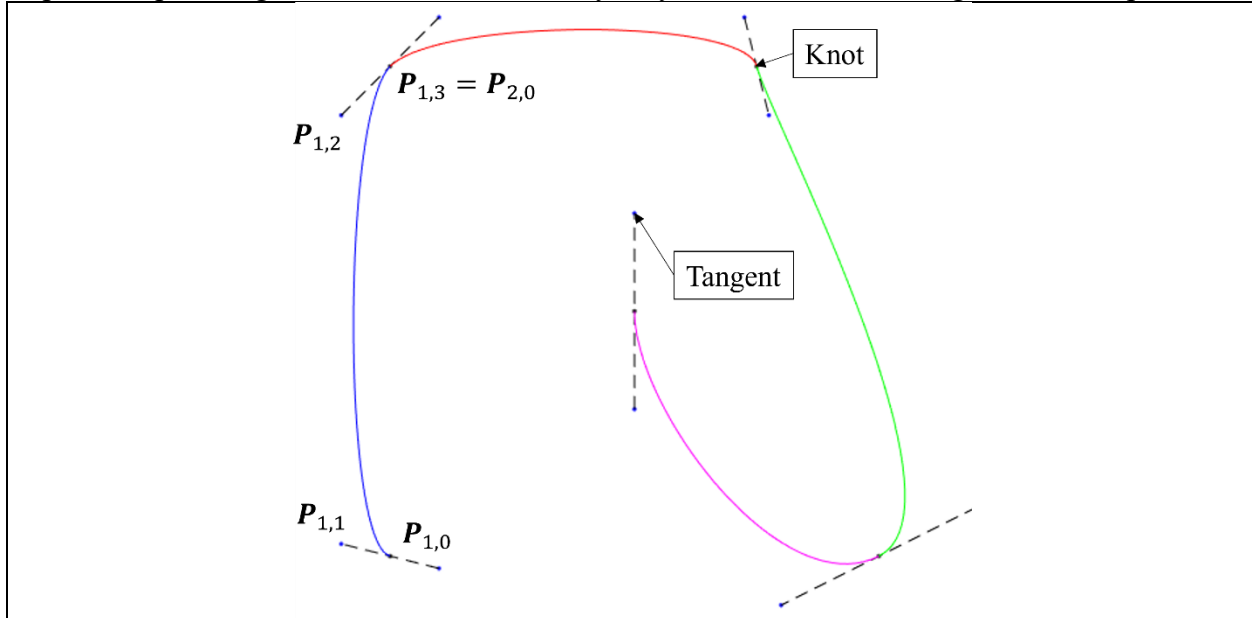


Figure 3. Example spline, with each segment assigned a different color. The spline clearly travels through the knot control points, whereas the tangent control points (end points of the dotted lines) denote the gradients but are not necessarily traveled through.

Continuity guarantees can be easily ensured between adjacent segments.  $C^1$  continuity can be enforced by constraining the tangent directions on either side of a knot (i.e., the dotted lines in Figure 3). The directions of these vectors should be equal and opposite, but their magnitudes do not necessarily need to be the same. For this reason, it is useful to reparameterize the spline as:

$\mathbf{x}_i(t) = (1 - t)^3 \mathbf{P}_i + 3(1 - t)^2 t \mathbf{T}_i^+ + 3(1 - t) t^2 \mathbf{T}_i^- + t^3 \mathbf{P}_{i+1} \text{ where } 0 \leq t \leq 1$ $\mathbf{T}_i^\pm = \mathbf{P}_i \pm d_i^\pm \hat{n}_i$	(2)
--	-----

$\mathbf{T}_i^\pm$  are the tangent points (i.e.,  $\mathbf{P}_{i,1}$  and  $\mathbf{P}_{i,2}$ ), which are defined relative to their adjacent knot and a (1) tangent direction ( $\hat{n}_i$ ) and (2) magnitude ( $d_i^\pm$ ) that is allowed to vary on the two opposing sides. This parameterization guarantees  $C^1$  continuity, which is extremely beneficial in the context of CFR materials, where smooth turning is critical for fiber health. In fact, radius of curvature ( $r$ ) can be explicitly calculated along the length of a spline by Equation 3.

$\kappa_i(t) = \frac{\det(\mathbf{x}'_i(t), \mathbf{x}''_i(t))}{\ \mathbf{x}'_i(t)\ ^3}$ $r_i(t) = \kappa_i^{-1}(t)$	(3)
--	-----

This parameterization of the toolpath imparts the following advantages:

1. **Local control of shape.** Moving control points within a specific segment only changes that segment (except knots, which change both of their adjacent segments). In contrast to other spline parameterizations whose control points have global effects (e.g., b-splines), the local control of Bézier splines makes them much easier to locate manually (and algorithmically).

2. **Continuity guarantees from tangent control points.** As mentioned above, simple constraints can be applied between adjacent spline segments to guarantee degrees of continuity. As a result, the splines are inherently smooth.
3. **Curvature is easily calculated.** Especially for CFR materials, turning radius is important to monitor within the toolpath. As defined in Equation (3), curvature is simple and fast to calculate along the length of a spline. A constraint can be formed to ensure all splines have at least some minimum radius of curvature.

## 2.2. Formation of Spline Families

Depending on the size of the geometry, a large number of splines may be necessary to cover each layer. Local variation in curvature also presents the same problems faced by the discussed integration schemes. To (1) maintain consistent toolpath spacing in a local region and (2) consolidate the variables available to the user (and optimization function), this work proposes the formation and use of spline “families.” These families are offset curves constructed from the same set of control points (Figure 4). When moving a control point on the root spline (i.e., the 0 offset), the corresponding control points in all of the offsets are moved as well.

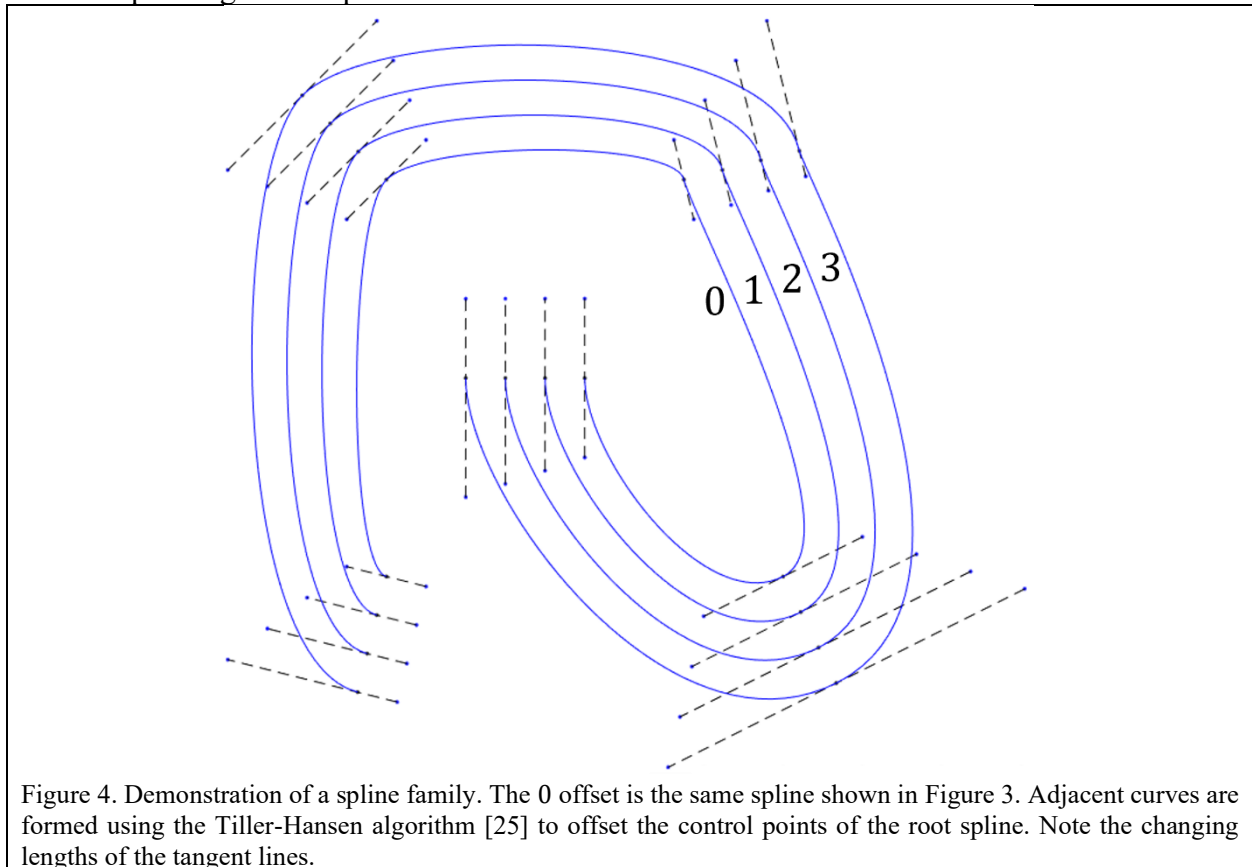
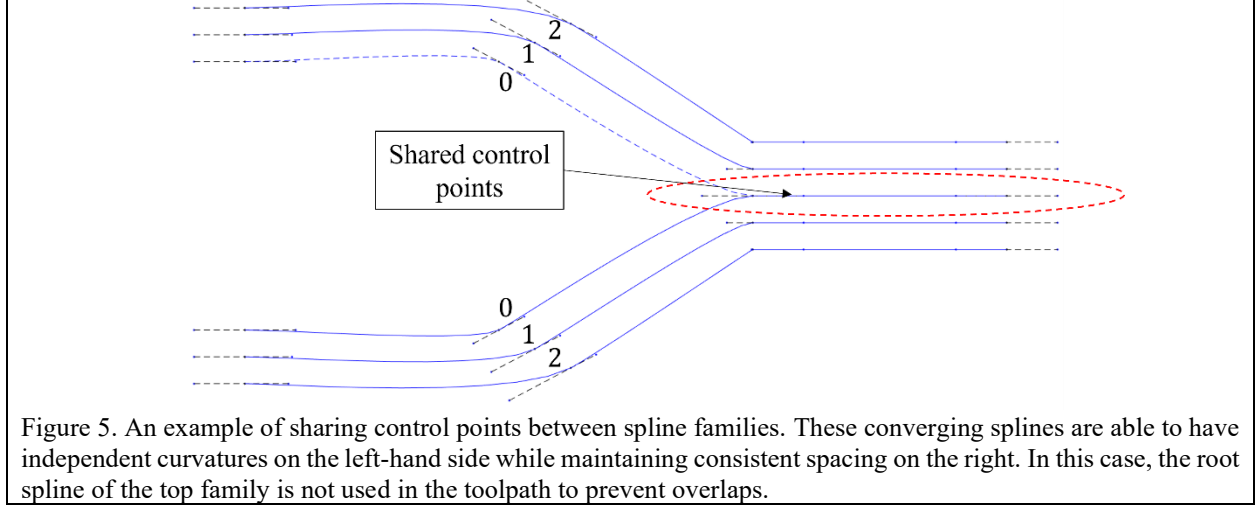


Figure 4. Demonstration of a spline family. The 0 offset is the same spline shown in Figure 3. Adjacent curves are formed using the Tiller-Hansen algorithm [25] to offset the control points of the root spline. Note the changing lengths of the tangent lines.

Further, it may be desirable to share control points between spline families. This enables independent motion in regions with different curvature but maintains consistent spacing in converging regions (e.g., truss intersections). An example is shown in Figure 5; the spline segments between the shared control points will inherently have the same local curvature. This also reduces the degrees of freedom needing to be managed by the user or optimized during the fitting process.



### 2.3. Optimization of Spline Fit

Once the user has laid out the initial spline families, they can be fit to the input orientation field. This is done by solving the optimization problem shown in Equation 4. Note that the optimization problem is unaware of the geometric boundaries. Side constraints could be applied to ensure the control points stay within the design space if deemed necessary, but this was not implemented in the present work.

$\begin{aligned} & \min_{\mathbf{P}, \hat{\mathbf{n}}, \mathbf{d}^\pm} -f \\ & \text{Subject to:} \\ & g_i \leq 0 \quad \forall i \in N_F \end{aligned}$	(4)
--	-----

$\mathbf{P}$  is the set of knot control point locations,  $\hat{\mathbf{n}}$  is the set of tangent unit vectors, and  $\mathbf{d}^\pm$  is the set of tangent vector magnitudes (all as defined in Equation 2).  $f$  is the objective function comparing the direction of the local orientation field to the splines (Equation 5), and  $g_i$  is the constraint function imposing a minimum fiber turning radius on spline family  $i$  (Equation 6).

$f = \frac{\sum_{i \in N_F} \sum_{j \in N_{O,i}} \sum_{k \in N_{S,i,j}} \left\  \frac{x'_{i,j,k}(t)}{\ x'_{i,j,k}(t)\ } \cdot v(x_{i,j,k}(t)) \right\ }{\sum_{i \in N_F} \sum_{j \in N_{O,i}} N_{S,i,j}}$	(5)
---	-----

$N_F$  is the number of spline families,  $N_{O,i}$  is the number of offsets in family  $i$ , and  $N_{S,i,j}$  is the number of segments in offset  $j$ . The equation takes the dot product of the normalized spline direction and the orientation field at that location. Each product is on the range  $[-1,1]$ . The absolute value handles the rotational symmetry in the orientation field; a specific path printed from either direction has the same performance. For instance, a prescribed road direction aligned to the  $45^\circ$  direction is equivalent to a prescribed direction of  $225^\circ$ . Therefore, each summand (and  $f$ ) is on the range  $[0,1]$ , where 1 represents perfect alignment between the spline and the prescribed orientation field. This is then normalized by the number of samples such that  $f$  is also on the range  $[0,1]$ .

To ensure the toolpath obeys a minimum turning radius, an additional constraint is imposed on each spline family during optimization:

$g_i = \min(\kappa_{i,j,k}^{-1}(t) \forall j \in N_{O,i} \text{ and } k \in N_{S,i,j}) - r_{\min}$	(6)
--	-----

$r_{\min}$  is the minimum turning radius of the material, and  $\kappa$  is defined in Equation 2.

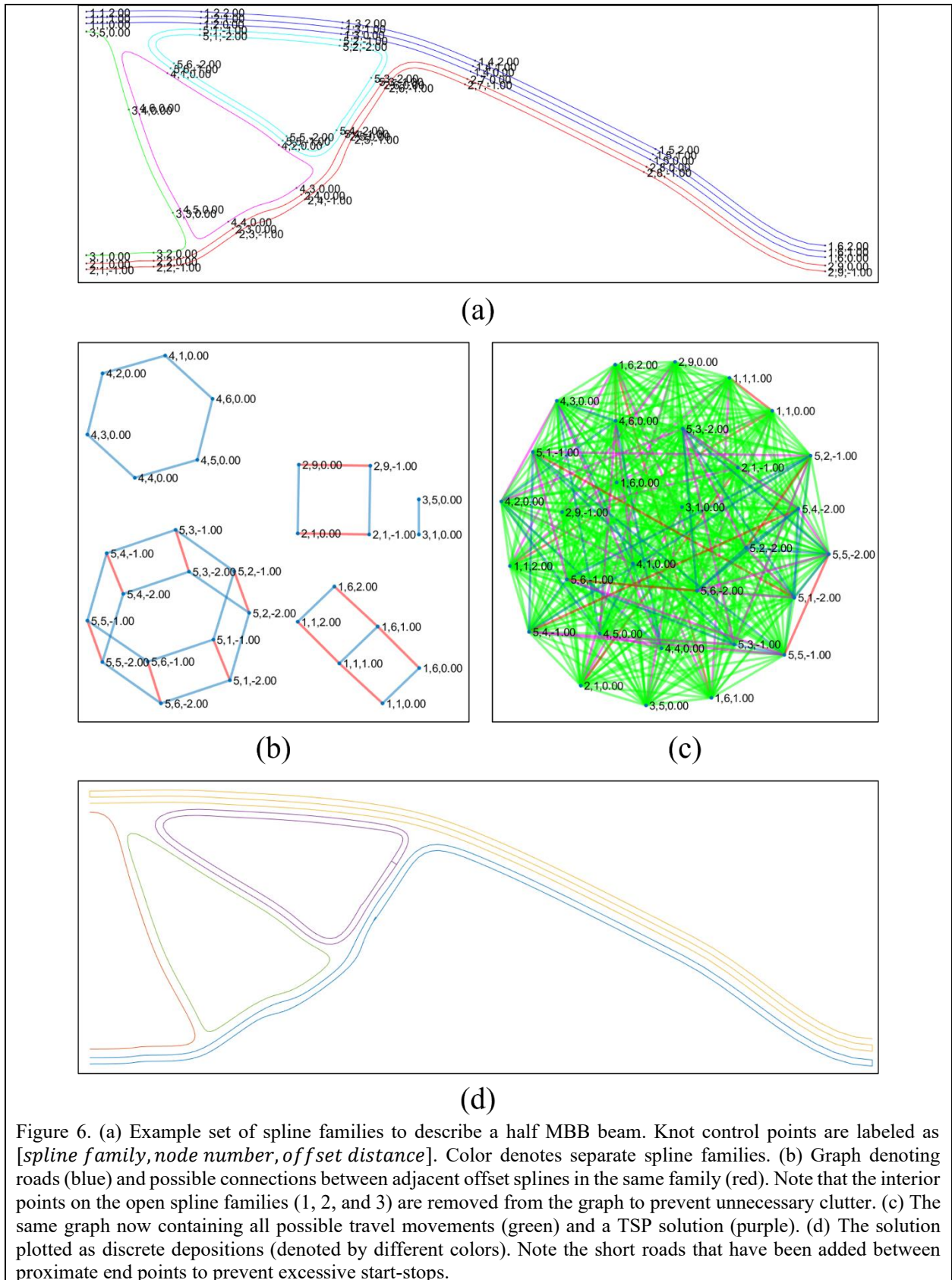
## 2.4. Ordering Splines to Maximize Fiber Length

Once the user is satisfied with the shape of the toolpath (either through additional editing or optimization), the splines need to be ordered within each layer for printing. This can be accomplished by (1) placing the control points on a graph as nodes and (2) connecting those nodes to describe roads and possible travel movements (Figure 6). The graph can then be traversed using the traveling salesman problem (TSP) [26] to form a printing order. However, naively offering the algorithm every travel movement option (Figure 6c) can result in suboptimal results. Especially for CFR materials, the toolpath should:

1. **Minimize the number of travel movements.** Each travel movement corresponds to a start-stop command for the extruder. For the deposition of CFR materials, this also requires a fiber cutting operation. This slows down the print and is a point of failure for many tools [27].
2. **Minimize the total travel distance.** For the sake of reducing print time, it is desirable to minimize the non-printing time for the deposition tool.

The example shown in Figure 6d requires five cut operations to achieve, when the design should intuitively only require two. To drive the algorithm towards these more optimal solutions, edges that describe known-suboptimal travel movements are trimmed from the graph. More specifically, the full list of control points is trimmed to a set of viable travel locations that meet at least one of the following criteria:

1. **Open splines.** Roads can optimally start from either end point of an open spline (Figure 7a).
2. **Closed spline with shared control points.** If a control point on a closed spline is shared with another closed spline family, this represents a possible transition location between the two families. If for instance, the deposition started at a different point (e.g., the purple path in Figure 6d), the path would have to unnecessarily terminate. Therefore, only the control points shared between two closed spline families are added. Further, only the control points on the most-offset (relative to the root) spline are added to the travel list, as it will always be possible to transition to the more interior offsets (Figure 7b).
3. **Closed spline with no shared control points.** In the case that a closed spline family shares no control points with another closed spline family, all of the control points (on the furthest offset) are added to the viable travel list (Figure 7c).



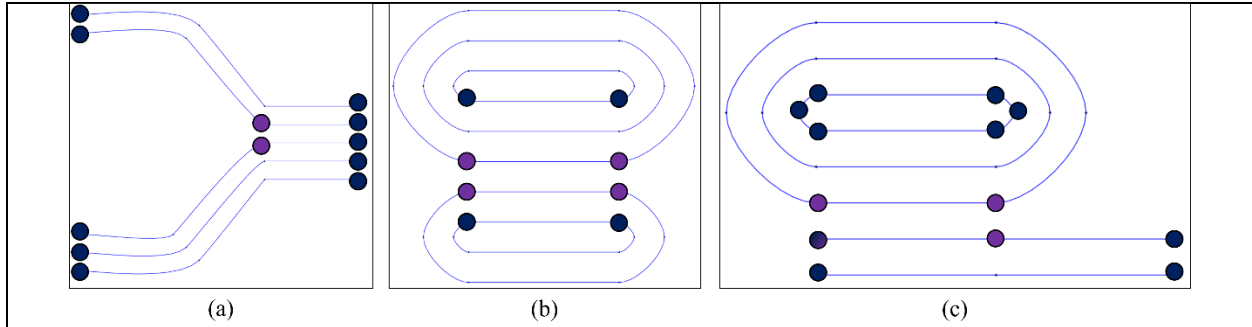
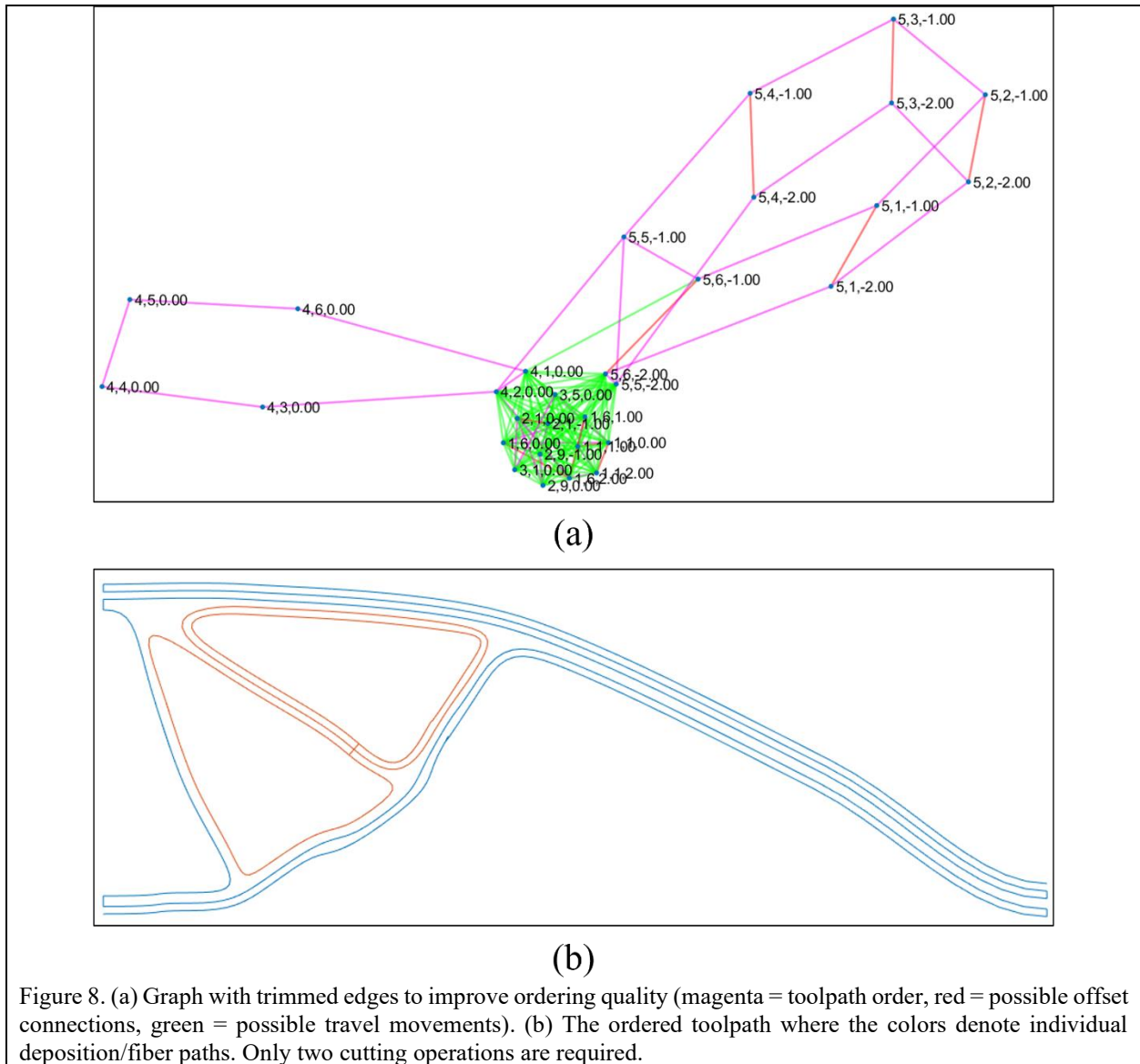


Figure 7. Examples of how shared control points (purple) are used to intelligently select viable travel movements (blue). (a) Both end points of an open spline are valid travel locations regardless of sharing. (b) In a closed spline with control points shared by another closed spline, only the most-offset nodes associated with the shared nodes are viable. (c) However, if the control points are shared with an open spline or the closed spline has no shared control points, all of the control points on the most-offset spline are listed as viable travel locations.

Using the graph of the control points with edges denoting possible connections between neighboring offset (Figure 6c), edges describing possible travel motions are added between all of the viable travel nodes found using the above criteria. Weights are assigned using the distances between the nodes. To properly set priority for the TSP algorithm, a weight of -1 is assigned to all edges describing roads, and a weight of 0 is assigned to all edges describing connections to adjacent offsets (blue and red edges in Figure 6c, respectively).

For this work, a greedy TSP algorithm was used that simply selected the lowest-cost edge that led to an unvisited node. The associated solution is shown in Figure 8a. The filtering criteria significantly reduced the number of edges in the graph (for the Messerschmitt-Bölkow-Blohm (MBB) beam example, from 435 to 144 edges). Removing the known-suboptimal edges also created a much better toolpath, reducing the number of required fiber cuts from five to two as shown in Figure 8b.

After ordering the control points, each spline offset can be interpolated following the graph traversal order. These interpolations can then be converted to GCode with appropriate extrusion/travel speeds and extrusion rates as prescribed by a process parameter file.



### 3. Implementation and Demonstration

To demonstrate the presented spline-based toolpath planning method, a user environment was created in Unity. A free utility (Dreamteck Splines [28]) was used for drawing and controlling splines that also contained functionality to share control points between families (Figure 9).

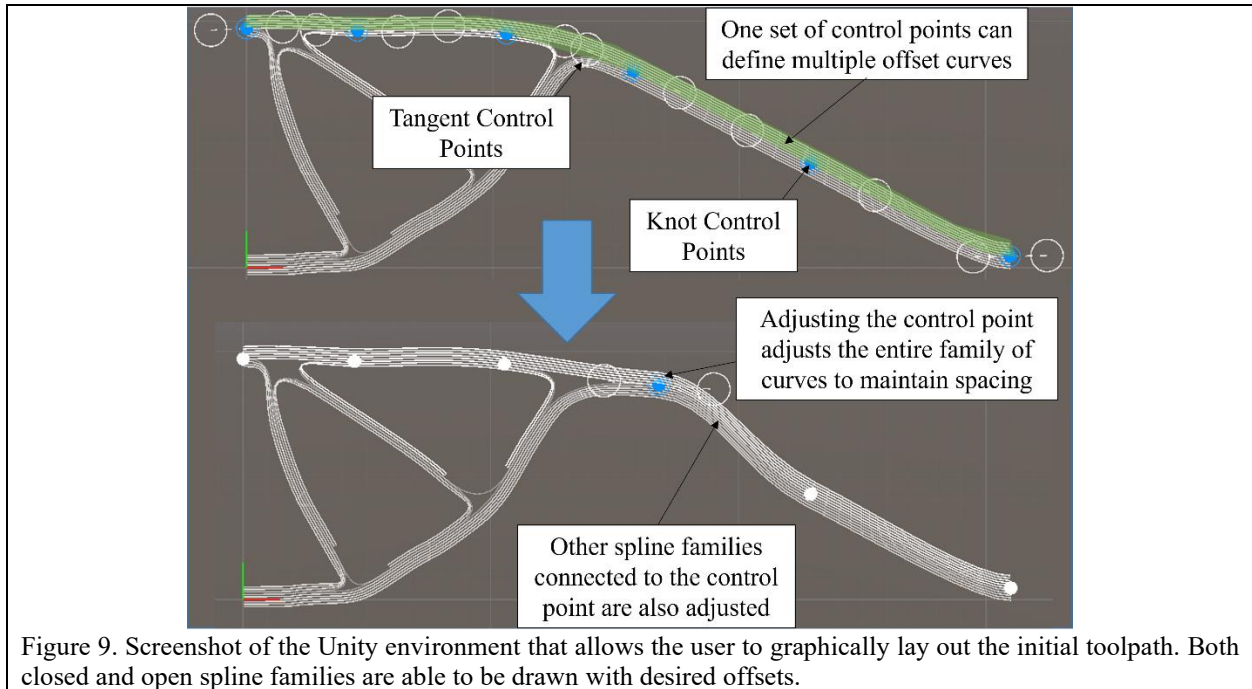


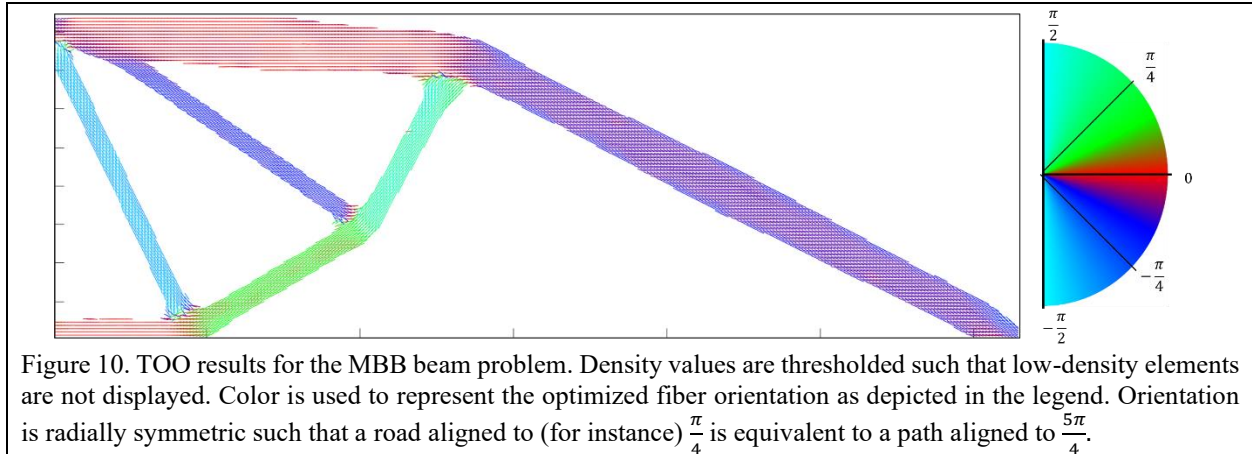
Figure 9. Screenshot of the Unity environment that allows the user to graphically lay out the initial toolpath. Both closed and open spline families are able to be drawn with desired offsets.

A desired geometry and orientation field can be overlaid during spline creation to allow the user to interpret critical features for manufacturability. At this stage, the user can identify offset distance (e.g., the road spacing dictated by their deposition platform) and count. Once satisfied, the fit of the spline families is optimized with respect to the orientation field.

To demonstrate these capabilities, an MBB problem was optimized using a topology and orientation optimization (TOO) algorithm to create a nominal geometry and orientation field [24]. From these inputs, a splines-based toolpath was created using the described workflow. For comparison, the same inputs were used to create toolpaths using existing alignment-based techniques (streamlines and analytic integration). These toolpaths are then compared qualitatively relative to the nominal geometry and quantitatively in terms of (1) alignment to the orientation field and (2) number of discrete fiber paths.

### 3.1. Topology and Orientation Optimization

Candidate inputs for the presented toolpath planning algorithm were generated via a TOO problem that simultaneously distributes and orients an anisotropic material to minimize structural compliance [24]. The results for an MBB problem are shown in Figure 10. Density is thresholded such that low density elements are not displayed. Pixel color instead represents the prescribed deposition direction (i.e., fiber orientation). As shown, fiber direction generally follows the truss direction.



### 3.2. Splines Toolpath Generation

Splines families were manually drawn in a custom Unity environment to approximately fill the optimized design as shown in Figure 11. Only 16 control points (and their associated tangents) across five spline families were required to describe the desired roads. To represent the symmetry across the central plane, the tangent directions of the associated control points were fixed to be aligned to the X-axis during optimization. A similar constraint was placed on the right-hand side to guarantee alignment of the open spline edges for easier rastering.

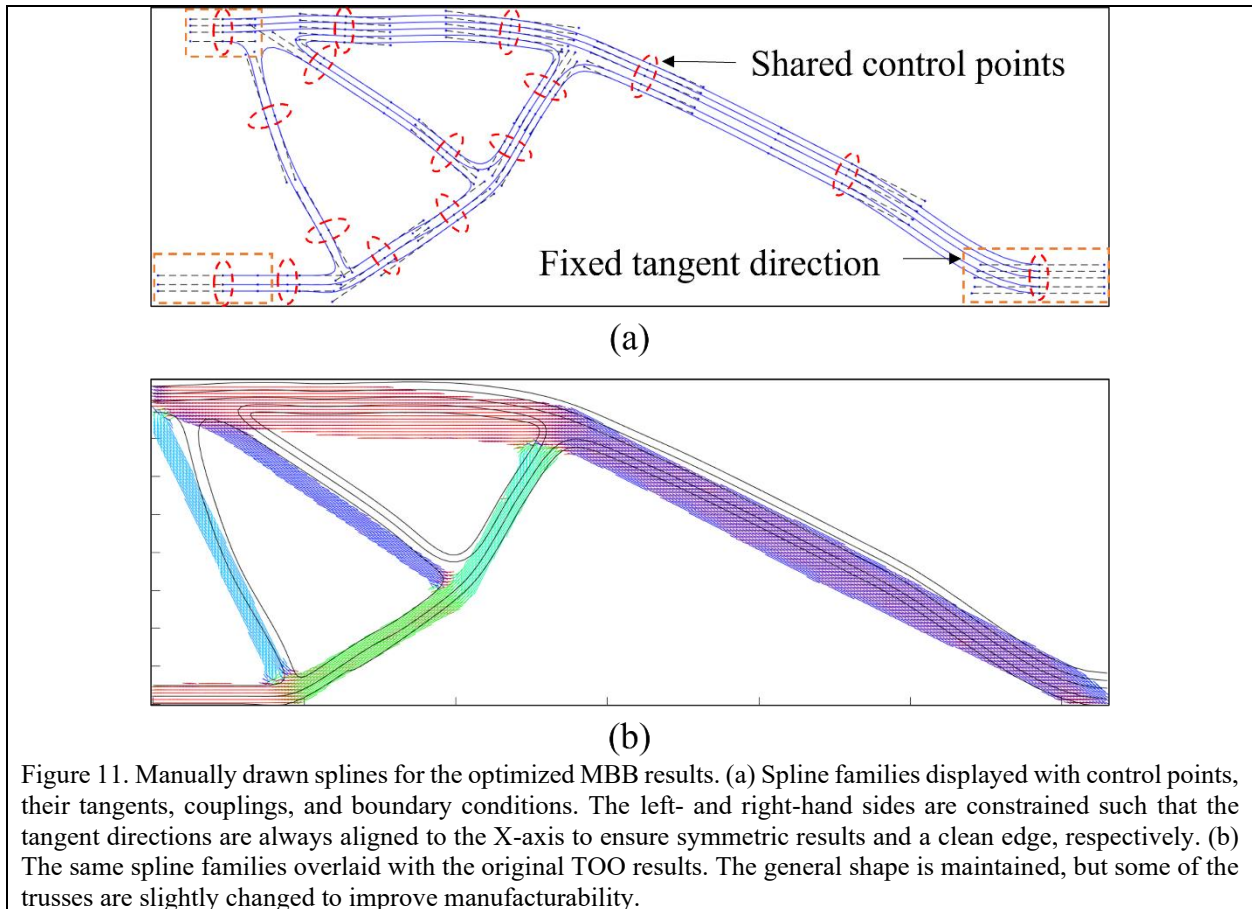


Figure 11. Manually drawn splines for the optimized MBB results. (a) Spline families displayed with control points, their tangents, couplings, and boundary conditions. The left- and right-hand sides are constrained such that the tangent directions are always aligned to the X-axis to ensure symmetric results and a clean edge, respectively. (b) The same spline families overlaid with the original TOO results. The general shape is maintained, but some of the trusses are slightly changed to improve manufacturability.

The splines are overlaid with the TOO results in Figure 11b. Slight deviations to the supporting trusses were used to improve curvature on the left-hand side; the light blue truss was too steep as-optimized for roads to properly merge with the primary truss.

The spline families were then fit to the optimized orientation field. When directly output from the TOO algorithm, the orientation field can have significant discontinuities in low density regions. The gradient-based optimization often ignores their impact and leaves them in unoptimized orientations. To ensure that the orientation field near each truss member was relevant, a nearest-neighbor interpolation was used to fill the thresholded areas (Figure 12a).

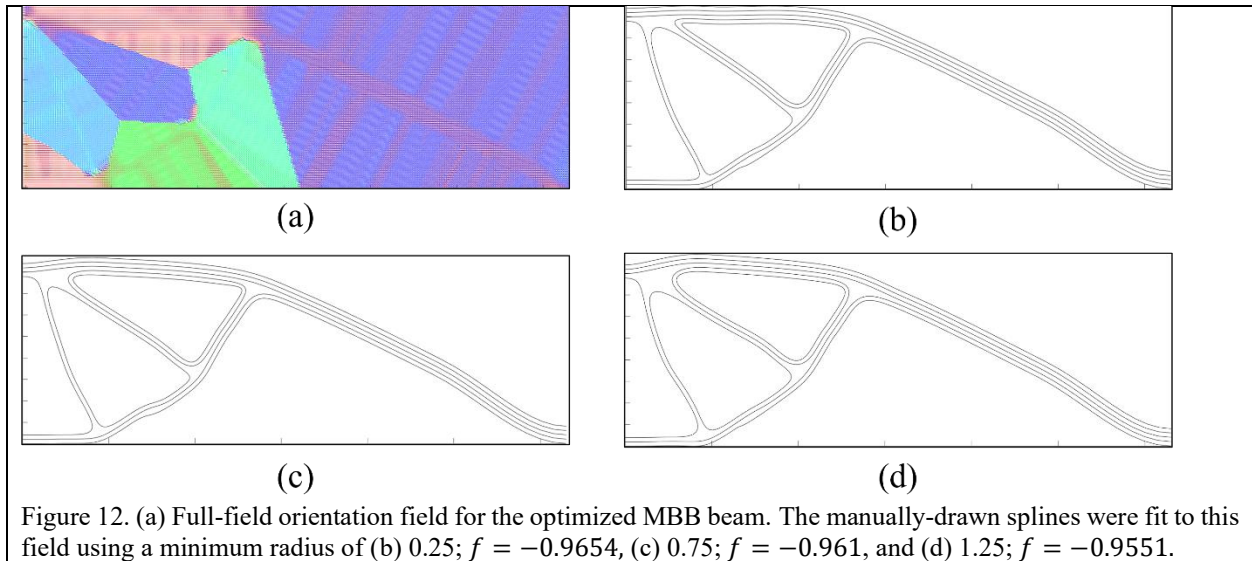


Figure 12 shows the results of the spline fitting using a variety of minimum fiber turning radii. Clearly, the deflections in the splines (especially the top-most primary truss member) increase with the turning radius constraint. It produces smoother splines but results in a lower fit. Perhaps more critically, even with a relatively small constraint (e.g.,  $r_{min} = 0.25$ ), gaps are produced between different spline families in converging truss members. This could perhaps be improved with a larger number of control points, but this would also increase computational expense. This issue is similar to that experienced in conventional contour-based toolpath planning [13]; however, contour toolpaths are often combined with uni-directional raster infill to specifically address these gaps. This type of infill would likely be unmanufacturable with CFR materials. Instead, (1) other spline configurations may need to be explored (e.g., alternating between a few different configurations across subsequent layers) or (2) inclusion of unreinforced material in those regions may be sufficient to direct load around the gaps. These opportunities will be explored as an aspect of future work.

### 3.3. Comparison to Other Alignment-Based Toolpath Planning Methods

Toolpaths for the optimized MBB geometry and orientation field were also planned using streamlines-based [13] and analytic integration (i.e., Poisson equation [20]) approaches. The resulting toolpaths are shown in Figure 13. It may be possible to link some proximate roads together to form more continuous raster patterns, but the notion of adjacency is less strict in these toolpath planning algorithms. Too large of a search radius could result in overlapping roads, which may cause the printing process to fail.

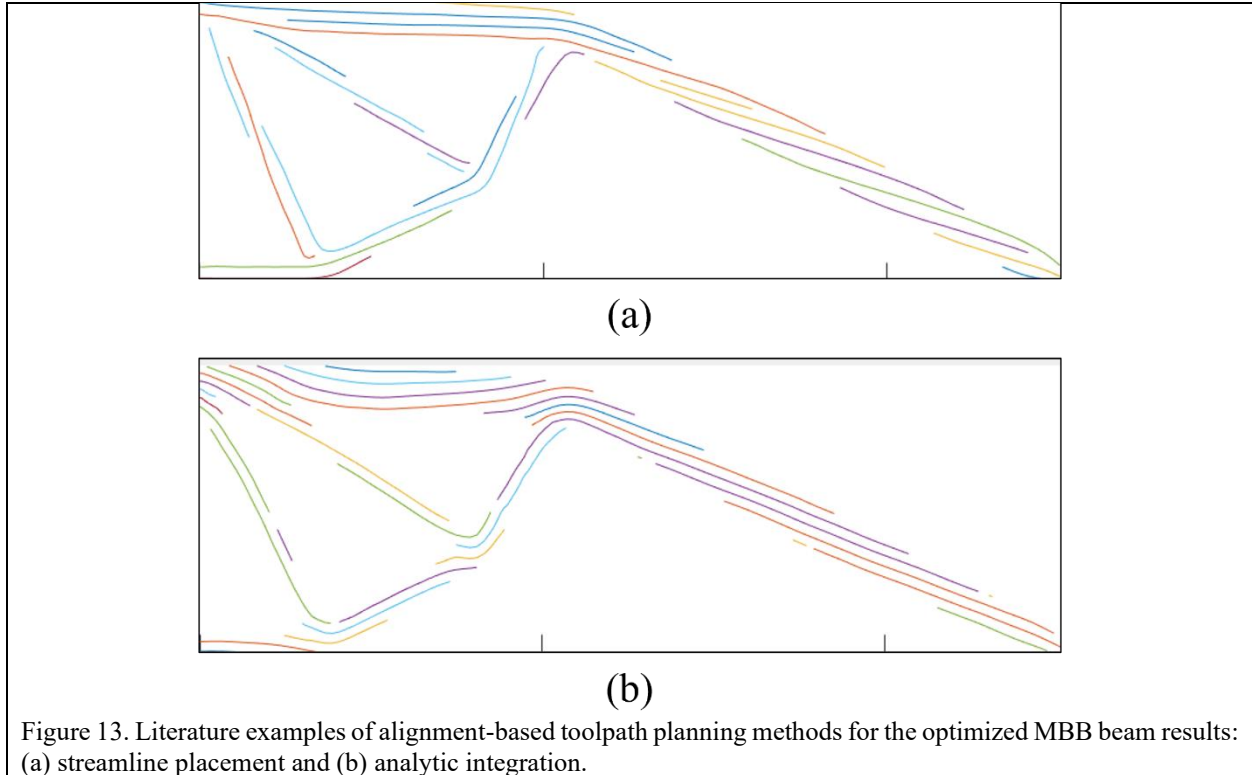


Figure 13. Literature examples of alignment-based toolpath planning methods for the optimized MBB beam results: (a) streamline placement and (b) analytic integration.

With these methods, a significantly larger number of discrete roads are required to fabricate the toolpath. As previously discussed, the splines-based toolpath only requires two discrete depositions, whereas the streamlines and analytic integration methods required 22 and 29 discrete paths, respectively. As can be seen, especially in Figure 13b, a significant number of roads are nearly connected, but they just cross out of the geometry's boundaries. In other areas (specifically, the secondary truss members of the streamlines toolpath), there is very poor continuity of roads through thin truss members. In conjunction, these deficiencies will likely significantly reduce mechanical performance.

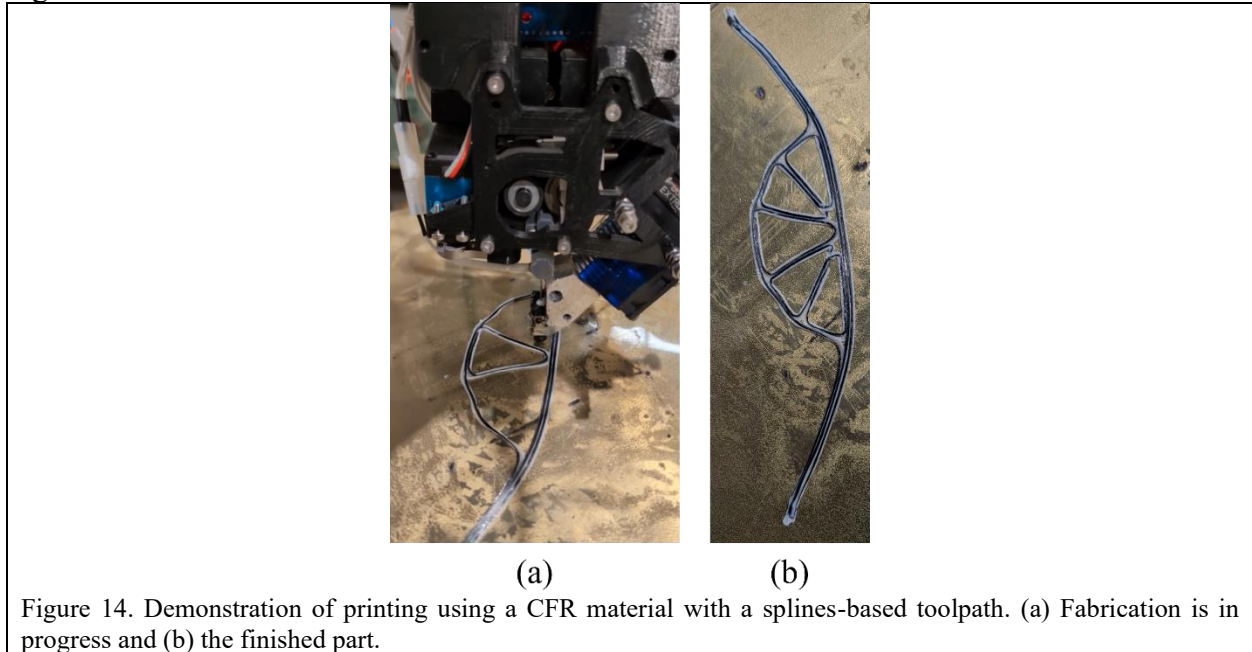
From an alignment perspective, the streamlines toolpath had an objective function value of  $f = -0.9873$ , which is slightly improved over the spline-based toolpath. On the other hand, the analytic integration toolpath has a value of  $f = -0.7569$ . This marked decrease in alignment quality is likely due (as previously discussed) to an overall non-conservative vector field. These are not uncommon in orientation fields (whether TOO or principal stresses), as they are not constrained by the physics of actual flow fields.

Overall, the splines-based toolpath has a slightly reduced alignment (relative to the streamlines-based toolpath). However, it significantly reduces the number of discrete depositions. It also offers improved continuity between truss members, reducing potential failure locations. At the same time, the gaps between different spline families (i.e., in truss intersections) may be an issue; preliminary mechanical testing has not yet been performed but will be as a point of future work.

### 3.4. Preliminary Printing Results

To demonstrate the splines-based toolpath as a potential solution for CFR material systems, a variant of the MBB beam toolpath was printed using a thermoplastic co-extrusion tool (tool design detailed in [5]). The splines were mirrored across the central plane to form the complete structure,

which ultimately required four discrete depositions to fabricate. The printed structure is shown in Figure 14.



The fiber had little issue with articulating the corners around the closed splines. However, the start of the fiber deposition was often slightly delayed, leading to a small gap in some of the paths. This may be improved with some randomization/alternation of start points between layers to prevent the development of a predominant seam in the final part. Alternatively, other patterns of splines that are qualitatively different may be alternated between layers to reduce dependence on any specific failure region.

#### 4. Summary

Toolpath alignment is important for AM processes, especially MEX. Material anisotropy (e.g., fiber) is ideally aligned to the anticipated load paths throughout a structure. Unfortunately, toolpath planning capabilities to leverage this aspect of the process are largely unavailable. Existing methods (1) result in poor path alignment or (2) create inconsistent spacing between paths. This paper addresses this gap via a novel toolpath planning workflow based on cubic Bézier splines, which inherently possess many of the characteristics of a high-quality toolpath: (1) continuity, (2) smooth curvature, (3) consistent spacing, and (4) ability to locally tailor toolpath orientation.

A workflow is presented that enables users to interactively draw a preliminary toolpath comprised of spline “families” (i.e., offset curves that derive from the same root set of control points). These families are then able to be fit to the anticipated load paths (i.e., an orientation field) to improve alignment. Due to the mathematical framing of the toolpath, this fitting process can be done under a minimum turning radius constraint to improve performance in the context of CFR materials. After fitting, the splines are connected and ordered for printing such that a minimal number of cuts is required.

A splines-based toolpath was then discussed in comparison to streamline and analytic integration toolpaths of the same geometry. Due to the increased freedoms of the splines-based toolpath (i.e., not being rigidly constrained to the boundaries of the geometry), a significant improvement in toolpath continuity was achieved. The toolpath also had nearly equivalent alignment to the orientation field as the streamlines toolpath (which was explicitly aligned to the

orientation field via the integration scheme). Preliminary demonstration of manufacturing with a CFR material was then conducted. The fiber was well-placed within the structure, though some effort may be required to improve strength in the regions where spline families change curvature (e.g., convergent truss regions).

#### 4.1. Future Work

This preliminary work offers significant opportunities for future work. In addition to characterizing the mechanical performance in comparison to benchmark toolpath planning processes, there is an opportunity to improve the quality of the splines-based toolpaths. For instance, fiber cutting could be better accounted for during the ordering process; after cutting, the minimum turning radius for the fiber dramatically increases [5]. Incorporating this into the identification of viable travel motions could dictate directionality around (for instance) closed splines to improve fiber health while increasing geometric flexibility. Other opportunities include automatic seeding of initial spline families to reduce the burden on the user. The concept of spline-based toolpaths could also be extended to the intersection of orthogonal Bézier surfaces to form non-planar toolpaths for use with multi-axis (i.e., robotic) MEX.

### 5. Acknowledgements

The author would like to thank Yasir Alsharif for printing the CFR sample shown in Figure 14.

### References

- [1] N. S. Hmeidat, B. Brown, X. Jia, N. Vermaak, and B. Compton, “Effects of infill patterns on the strength and stiffness of 3D printed topologically optimized geometries,” *Rapid Prototyp. J.*, vol. ahead-of-p, no. ahead-of-print, 2021, doi: 10.1108/rpj-11-2019-0290.
- [2] J. E. Seppala and K. D. Migler, “Infrared thermography of welding zones produced by polymer extrusion additive manufacturing,” *Addit. Manuf.*, vol. 12, no. October, pp. 71–76, 2016, doi: 10.1016/j.addma.2016.06.007.
- [3] S.-H. Ahn, M. Montero, D. Odell, S. Roundy, and P. K. Wright, “Anisotropic material properties of fused deposition modeling ABS,” *Rapid Prototyp. J.*, vol. 8, no. 4, pp. 248–257, 2002.
- [4] B. G. Compton and J. A. Lewis, “3D-Printing of Lightweight Cellular Composites,” *Adv. Mater.*, no. 26, pp. 5930–5935, 2014, doi: 10.1002/adma.201401804.
- [5] K. D. Beaumont, J. R. Kubalak, and C. B. Williams, “Multi-axis material extrusion of continuous carbon fiber composites: tool design and mechanical characterization,” *Int. J. Adv. Manuf. Technol.*, no. 0123456789, 2025, doi: 10.1007/s00170-025-15749-8.
- [6] M. P. Schmidt, L. Couret, C. Gout, and C. B. W. Pedersen, “Structural topology optimization with smoothly varying fiber orientations,” *Struct. Multidiscip. Optim.*, vol. 62, no. 6, pp. 3105–3126, 2020, doi: 10.1007/s00158-020-02657-6.
- [7] R. Rezaie, M. Badrossamay, a. Ghaie, and H. Moosavi, “Topology optimization for fused deposition modeling process,” *Procedia CIRP*, vol. 6, pp. 521–526, 2013, doi: 10.1016/j.procir.2013.03.098.
- [8] D. Li, W. Liao, N. Dai, G. Dong, Y. Tang, and Y. M. Xie, “Optimal design and modeling of gyroid-based functionally graded cellular structures for additive manufacturing,” *CAD Comput. Aided Des.*, vol. 104, pp. 87–99, 2018, doi: 10.1016/j.cad.2018.06.003.
- [9] A. M. M. Nazmul Ahsan and B. Khoda, “Characterizing Novel Honeycomb Infill Pattern for Additive Manufacturing,” *J. Manuf. Sci. Eng. Trans. ASME*, vol. 143, no. 2, Feb. 2021, doi: 10.1115/1.4048044.

- [10] H. Zhang, Y. Yao, Y. Ma, M. Lackner, and Y. Jiang, “A 3D printing tool-path generation strategy based on the partition of principal stress field for fused filament fabrication,” *Int. J. Adv. Manuf. Technol.*, 2022, doi: 10.1007/s00170-022-09957-9.
- [11] J. Wu, N. Aage, R. Westermann, and O. Sigmund, “Infill Optimization for Additive Manufacturing-Approaching Bone-Like Porous Structures,” *IEEE Trans. Vis. Comput. Graph.*, vol. 24, no. 2, pp. 1127–1140, 2018, doi: 10.1109/TVCG.2017.2655523.
- [12] G. Liu *et al.*, “Stress field-aware infill toolpath generation for additive manufacturing of continuous fiber reinforced polymer composites,” *Mater. Des.*, vol. 239, no. February, p. 112756, 2024, doi: 10.1016/j.matdes.2024.112756.
- [13] J. R. Kubalak, N. J. Root, A. L. Wicks, and C. B. Williams, “Improving mechanical performance in material extrusion parts via optimized toolpath planning,” *Addit. Manuf.*, vol. 80, no. September 2022, p. 103950, 2023, doi: 10.1016/j.addma.2023.103950.
- [14] J. R. Kubalak, A. L. Wicks, and C. B. Williams, “Simultaneous topology and toolpath optimization for layer-free multi-axis additive manufacturing of 3D composite structures,” *Addit. Manuf.*, vol. 104, no. April, p. 104774, 2025, doi: 10.1016/j.addma.2025.104774.
- [15] V. Murugan, G. Alaimo, F. Auricchio, and S. Marconi, “An Orientation-Field Based Algorithm for Free-Form Material Extrusion,” *Addit. Manuf.*, p. 103064, 2022, doi: 10.1016/j.addma.2022.103064.
- [16] T. R. Brooks and J. R. R. A. Martins, “On manufacturing constraints for tow-steered composite design optimization,” *Compos. Struct.*, vol. 204, no. August, pp. 548–559, 2018, doi: 10.1016/j.compstruct.2018.07.100.
- [17] M. Zmyślony, K. Dradrach, and J. S. Biggins, “Slicing vector fields into tool paths for additive manufacturing of nematic elastomers,” *Addit. Manuf.*, vol. 97, no. June 2024, p. 104604, 2025, doi: 10.1016/j.addma.2024.104604.
- [18] H. Ren, D. Wang, G. Liu, D. W. Rosen, and Y. Xiong, “Concurrent optimization of structural topology and toolpath for additive manufacturing of continuous fiber-reinforced polymer composites,” *Comput. Methods Appl. Mech. Eng.*, vol. 430, no. July, p. 117227, 2024, doi: 10.1016/j.cma.2024.117227.
- [19] N. Ichihara and M. Ueda, “3D-printed high-toughness composite structures by anisotropic topology optimization,” *Compos. Part B Eng.*, vol. 253, no. August 2022, p. 110572, 2023, doi: 10.1016/j.compositesb.2023.110572.
- [20] G. Fang, T. Zhang, S. Zhong, X. Chen, Z. Zhong, and C. C. L. Wang, “Reinforced FDM: Multi-Axis Filament Alignment with Controlled Anisotropic Strength,” in *ACM Trans. Graph.*, 2020, vol. 39, no. 6.
- [21] X. Guidetti, E. C. Balta, Y. Nagel, H. Yin, A. Rupenyan, and J. Lygeros, “Stress flow guided non-planar print trajectory optimization for additive manufacturing of anisotropic polymers,” *Addit. Manuf.*, vol. 72, no. January, p. 103628, 2023, doi: 10.1016/j.addma.2023.103628.
- [22] D. A. Jaffa, “Conservative Vector Fields and the Intersect Rule,” *J. Appl. Math. Phys.*, vol. 11, no. 10, pp. 2888–2903, 2023, doi: 10.4236/jamp.2023.1110190.
- [23] F. Wein, J. Mirbach, A. Angre, J. Greifenstein, and D. Hübner, “Multi-layer continuous carbon fiber pattern optimization and a spline based path planning interpretation,” *J. Manuf. Process.*, vol. 135, no. September 2024, pp. 375–387, 2024, doi: 10.1016/j.jmapro.2025.01.038.
- [24] J. R. Kubalak, A. L. Wicks, and C. B. Williams, “Investigation of Parameter Spaces for Topology Optimization with Three-Dimensional Orientation Fields for Multi-Axis Additive

- Manufacturing,” *J. Mech. Des.*, pp. 1–18, 2020, doi: 10.1115/1.4048117.
- [25] W. Tiller and E. G. Hanson, “Offsets of Two-Dimensional Profiles,” pp. 36–46, 1984.
- [26] G. Laporte, “The Traveling Salesman Problem: An overview of exact and approximate algorithms,” *Eur. J. Oper. Res.*, vol. 59, pp. 231–247, 1992.
- [27] W. de Backer, M. J. L. van Tooren, and A. P. Bergs, “Multi-axis multi-material fused filament fabrication with continuous fiber reinforcement,” *AIAA/ASCE/AHS/ASC Struct. Struct. Dyn. Mater. Conf. 2018*, no. 210049, 2018, doi: 10.2514/6.2018-0091.
- [28] Dreamteck, “Dreamteck Splines,” *Unity Asset Store*. [Online]. Available: <https://assetstore.unity.com/packages/tools/utilities/dreamteck-splines-61926>.